

Numerical analysis of center cracked orthotropic fgm plate: Crack and material axes differ by θ°

Mete Onur Kaman¹ and Fatih Cetisli*²

¹Firat University, Department of Mechanical Engineering, Elazig, Turkey

²Firat University, Department of Civil Engineering, Elazig, Turkey

(Received February 10, 2012, Revised May 07, 2012, Accepted May 17, 2012)

Abstract. In this study, fracture analysis of orthotropic FGM (Functionally Graded Material) plate having center crack is performed, numerically. Material axis arbitrarily oriented and there is an angle θ° between material and crack axes. Stress intensity factors at the crack tips for Mode I are calculated using *Displacement Correlation Method* (DCM). In numerical analysis, effects of material properties and variation of angle θ° between material and crack axes on the fracture behavior are investigated for four different boundary conditions. Consequently, it is found that the effect of θ° on stress intensity factor depends on variation of material properties.

Keywords: orthotropic functionally graded materials; displacement correlation method; finite element analysis; stress intensity factor; aerospace structures.

1. Introduction

Recently, application areas of Functionally Graded Materials (FGMs) rapidly increase in thermal barrier coating, wear and impact resistant, energy conversion, dental implant industry due to their advanced properties. FGMs are multi-phase materials in which the volume fractions of the constituents vary as a function of position, typically in the thickness direction (Ayhan 2007).

The microstructure of FGMs is generally heterogeneous, and the dominant type of failure in FGM is crack initiation and growth from inclusions (Rao and Rahman 2003). Given the nature of processing techniques for example plasma sprayed method, graded materials can become anisotropic. In order to take the material orientation into account in the fracture analyses, graded materials are generally modeled as orthotropic with principal directions parallel and perpendicular to the boundaries (Dag 2006). Chen *et al.* (2002) studied the transient internal crack problem for a functionally graded orthotropic strip. Integral transforms and dislocation density functions were employed to reduce the problem to singular integral equations. A theoretical treatment of mode I crack problem was put forward for a functionally graded orthotropic strip by Guo *et al.* (2004). The internal crack and edge crack perpendicular to the boundaries were investigated, respectively. The principal directions of orthotropy were parallel and perpendicular to the boundaries of the strip. The singular integral equation for solving the problem and the corresponding asymptotic expression of the singular kernel were

* Corresponding author, Assistant Professor, E-mail: fcetisli@firat.edu.tr

obtained. The plane strain problems of semi-infinite cracks in an infinite functionally graded orthotropic material were studied by Hongmin *et al.* (2008). Two uniform impact loading modes were considered, i.e., opening and in-plane shear. Closed form solutions of the dynamic stress intensity factors were obtained. It was observed that the stress intensity factors were not all proportional to the square root of time as expected. Kim and Paulino (2002a) developed a finite element methodology for fracture analysis of FGMs where cracks were arbitrarily oriented with respect to the principal axes of material orthotropy. Stress intensity factors (SIFs) for mode I and mixed-mode two-dimensional problems were evaluated and compared by means of the Modified Crack Closure (MCC) and the Displacement Correlation Method (DCM) especially tailored for orthotropic FGMs. Dag *et al.* (2007) examined mixed-mode fracture problems of FGMs under mechanical and thermal loading conditions. In the case of mechanical loading, an embedded crack in an orthotropic FGM layer was considered. An analytical solution based on the singular integral equations and a numerical approach based on the enriched finite elements were developed to evaluate the mixed-mode stress intensity factors and the energy release rate under the given mechanical loading conditions. Kim and Paulino (2003a) extended the concept to orthotropic functionally graded materials and addressed fracture mechanics problems with arbitrarily oriented straight and/or curved cracks. Stress intensity factors for mode I and mixed-mode two-dimensional problems were evaluated by means of the interaction integral and the finite element method. Quasi-static mixed mode stress fields for a crack in orthotropic inhomogeneous medium are developed using asymptotic analysis coupled with Westergaard stress function approach by Chalivendra (2009). Using the derived mixed-mode stress field equations, the isochromatic fringe contours were developed to understand the variation of stress field around the crack tip as a function of both orthotropic stiffness ratio and non-homogeneous coefficient. Zhou *et al.* (2007) investigated the transient thermal fracture problem of a crack (perpendicular to the gradient direction) in a graded orthotropic strip. Most of the materials properties were assumed to vary as an exponential function of thickness direction. The transient two-dimensional temperature problem was analyzed by the methods of Laplace and Fourier transformations. A system of singular integral equations was obtained and solved numerically.

The Boundary Element Method (BEM) and meshless methods have been successfully applied for crack problems in FGM with a general orientation for material gradation in 2-d and 3-d analyzes. The efficient interaction integral method for evaluation of stress intensity factors was also discussed in the literature (Gao *et al.* 2008, Sladek *et al.* 2008a, Sladek *et al.* 2008b)

In all studies mentioned above fracture mechanics analyses of orthotropic functionally graded materials are carried out that principle orthotropy axis is parallel or perpendicular to the boundaries of plate under mechanical loading. Since crack and material axes may be differ by an angle in graded coatings that are subjected to tensile loads in various applications, computational methods to calculate fracture mechanics parameters in orthotropic FGMs are also required.

The present study concerns fracture analysis of orthotropic FGM plate having center crack. Behavior of FGM plate is exponential. Material axis is oriented arbitrarily with respect to the crack axis and there is an angle θ° between principal material orthotropy (1 and 2) and crack axes. In the literature, material axis is taken as a constant value $\theta^{\circ} = 0^{\circ}$ or 90° and crack axis is changed from 0° to 90° (Dag 2006, Dag *et al.* 2007, Kim and Paulino 2002a, Kim and Paulino 2003a, Kim and Paulino 2003b, Kim and Paulino 2005, Rao and Rahman 2003). But in the present study, crack axis is constant ($\theta = 0^{\circ}$), material axis is changed from 0° to 90° . Stress intensity factors at the crack tips for Mode I are calculated using DCM. ANSYS 12.1 finite element package program is used to calculate displacements at the crack face. Gradient of material properties for FGM, boundary condition and numerical model are defined with the

help of a subroutine prepared by using APDL (*ANSYS Parametric Design Language*) codes. In the numerical analysis, effects of material properties and variation of angle θ° between material and crack axes on fracture behavior are investigated for four different boundary conditions.

2. Orthotropic FGM plate

This study investigates the fracture analysis of orthotropic FGMs and the effect of the θ° on stress intensity factors using the finite element method (Fig. 1). Material properties of orthotropic FGMs are defined as

$$E_{11}(x_1) = E_{11}^0 e^{\beta x_1} \quad (1)$$

$$E_{22}(x_1) = E_{22}^0 e^{\beta x_1} \quad (2)$$

$$G_{12}(x_1) = G_{12}^0 e^{\beta x_1} \quad (3)$$

where E_{11} , E_{22} and G_{12} are longitudinal, transverse and shear modulus of material, respectively. x_1 is the direction of material gradation and β is material nonhomogeneity parameter. On the other hand, the Poisson's ratio ν_{12} is assumed to be constant. If material properties in $x(x_1, x_2)$ (inclined by θ° with respect to the X_1 coordinate) are transformed to the global coordinate system $X(X_1, X_2)$, they can be obtained as (Kim and Paulino 2005)

$$E_{11}(X_1) = E_{11}^0 e^{(\phi_1 X_1 + \phi_2 X_2)} \quad (4)$$

$$E_{22}(X_1) = E_{22}^0 e^{(\phi_1 X_1 + \phi_2 X_2)} \quad (5)$$

$$G_{12}(X_1) = G_{12}^0 e^{(\phi_1 X_1 + \phi_2 X_2)} \quad (6)$$

where ϕ_1 and ϕ_2 are related by

$$\phi_1 = \beta \cos \theta, \quad \phi_2 = \beta \sin \theta \quad (7)$$

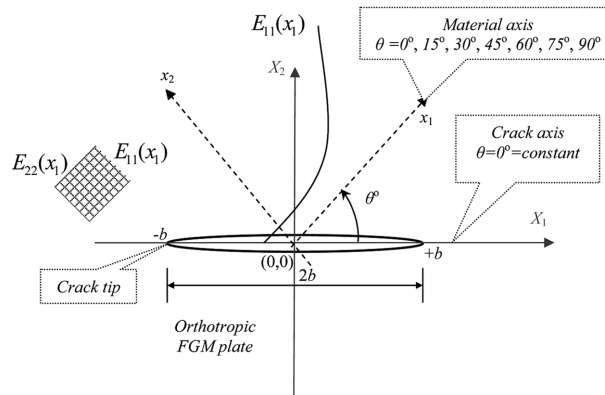


Fig 1 Geometry and notation for crack problems in an orthotropic FGM plate

For pure Mode I, the relationship between displacements and stress intensity factor (K_I) in the vicinity of the crack tip are (Kim and Paulino 2002a)

$$u_1 = K_I \sqrt{\frac{2r}{\pi}} \operatorname{Re} \left\{ \frac{1}{\mu_1^{tip} - \mu_2^{tip}} [\mu_1^{tip} p_2 \sqrt{\cos \alpha + \mu_2^{tip} \sin \alpha} - \mu_2^{tip} p_1 \sqrt{\cos \alpha + \mu_1^{tip} \sin \alpha}] \right\} \quad (8)$$

$$u_2 = K_I \sqrt{\frac{2r}{\pi}} \operatorname{Re} \left\{ \frac{1}{\mu_1^{tip} - \mu_2^{tip}} [\mu_1^{tip} q_2 \sqrt{\cos \alpha + \mu_2^{tip} \sin \alpha} - \mu_2^{tip} q_1 \sqrt{\cos \alpha + \mu_1^{tip} \sin \alpha}] \right\} \quad (9)$$

for polar coordinate system (r, α). Similarly, for pure Mode II, the relationships between displacements and stress intensity factor (K_{II}) in the vicinity of the crack tip are

$$u_1 = K_{II} \sqrt{\frac{2r}{\pi}} \operatorname{Re} \left\{ \frac{1}{\mu_1^{tip} - \mu_2^{tip}} [p_2 \sqrt{\cos \alpha + \mu_2^{tip} \sin \alpha} - p_1 \sqrt{\cos \alpha + \mu_1^{tip} \sin \alpha}] \right\} \quad (10)$$

$$u_2 = K_{II} \sqrt{\frac{2r}{\pi}} \operatorname{Re} \left\{ \frac{1}{\mu_1^{tip} - \mu_2^{tip}} [q_2 \sqrt{\cos \alpha + \mu_2^{tip} \sin \alpha} - q_1 \sqrt{\cos \alpha + \mu_1^{tip} \sin \alpha}] \right\} \quad (11)$$

In the above equations, μ_1^{tip} and μ_2^{tip} denote the Eigen values of the compatibility equations with positive imaginary part (Sills *et al.* 2005). μ_1^{tip} and μ_2^{tip} must be calculated at the location of a crack tip and global coordinate system $X(X_1, X_2)$ for FGMs.

$$S_{11}\mu^4 - 2S_{16}\mu^3 + (2S_{11} + S_{66})\mu^2 - S_{26}\mu + S_{22} = 0 \quad (12)$$

where S_{ij} 's ($i, j = 1, 2, 6$) are the compliance coefficients at the crack tip and can be written as

$$S_{ij} = \begin{bmatrix} S_{11} & S_{12} & 0 \\ S_{12} & S_{22} & 0 \\ 0 & 0 & S_{66} \end{bmatrix} = \begin{bmatrix} \frac{1}{E_{11}^{tip}} & -\frac{\nu_{21}}{E_{22}^{tip}} & 0 \\ -\frac{\nu_{12}}{E_{11}^{tip}} & \frac{1}{E_{22}^{tip}} & 0 \\ 0 & 0 & \frac{1}{G_{12}^{tip}} \end{bmatrix} \quad (13)$$

The strain-stress relationships of an orthotropic material in plane stress state can be given as

$$\begin{Bmatrix} \varepsilon_1 \\ \varepsilon_2 \\ \varepsilon_6 \end{Bmatrix} = \begin{bmatrix} S_{11} & S_{12} & 0 \\ S_{12} & S_{22} & 0 \\ 0 & 0 & S_{66} \end{bmatrix} \begin{Bmatrix} \sigma_1 \\ \sigma_2 \\ \sigma_6 \end{Bmatrix} \quad (14)$$

The independent engineering constants, namely compliance coefficients E_{11} , E_{22} and G_{12} are written

in terms of averaged Young modulus E as

$$E = \sqrt{E_{11}E_{12}} \quad (15)$$

the effective Poisson's ratio ν is written as

$$\nu = \sqrt{\nu_{12}\nu_{21}} \quad (16)$$

the stiffness ratio δ^4 is written as

$$\delta^4 = \frac{E_{11}}{E_{22}} = \frac{\nu_{12}}{\nu_{21}} \quad (17)$$

and the shear parameters κ_0 is written as

$$\kappa_0 = \frac{E}{2G_{12}} - \nu \quad (18)$$

for generalized plane stress (Kim and Paulino 2003b). These parameters assist to define orthotropic FGM properties, easily. Besides, p_k and q_k ($k = 1, 2$) are given by

$$p_k = S_{11}(\mu_k^{tip})^2 + S_{12} - S_{16}\mu_k^{tip} \quad (19)$$

$$q_k = S_{12}(\mu_k^{tip})^2 + \frac{S_{22}}{\mu_k^{tip}} - S_{26} \quad (20)$$

3. Numerical study

3.1 Displacement correlation method (DCM)

In order to obtain the stress intensity factor numerically, easy-applicable numerical method, DCM is used. For singular finite element model at the crack tip (Fig. 2), the Crack Opening Displacement (COD) and Crack Sliding Displacement (CSD) are given as follows (Kim and Paulino 2002a, Shih *et al.* 1976)

$$COD = \sqrt{\frac{r}{\Delta b}}(4\Delta v_{34} - \Delta v_{56}) = \sqrt{\frac{r}{\Delta b}}[4(v_3 - v_4) - (v_5 - v_6)] \quad (21)$$

$$COD = \sqrt{\frac{r}{\Delta b}}(4\Delta u_{34} - \Delta u_{56}) = \sqrt{\frac{r}{\Delta b}}[4(u_3 - u_4) - (u_5 - u_6)] \quad (22)$$

where b is crack length and Δb is the characteristic length of the quarter point crack tip elements. On the other hand, Δu_{34} , Δu_{56} , Δv_{34} and Δv_{56} are the relative displacements with respect to the crack tip in

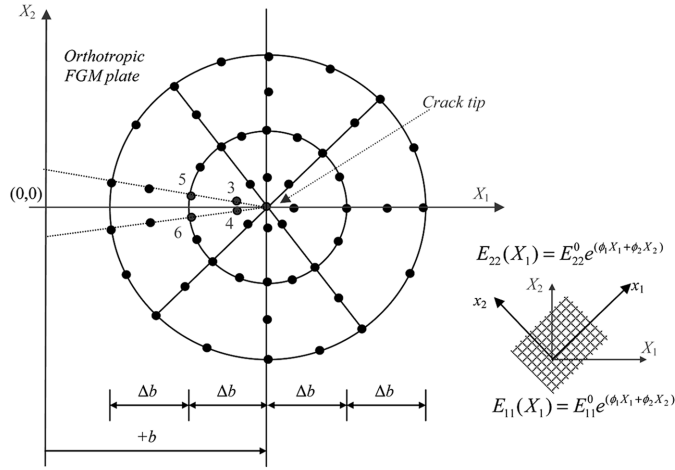


Fig 2 Finite element model at the crack tip

the X_1 and X_2 direction at locations as shown in Fig. 2. Displacements at the crack tip using Eqs. (8-11) can be written by combination of two modes K_I and K_{II} as

$$u_1 = K_I \sqrt{\frac{2r}{\pi}} \operatorname{Re} \left[\frac{i}{\mu_1 - \mu_2} (\mu_1 q_2 - \mu_2 q_1) \right] + K_{II} \sqrt{\frac{2r}{\pi}} \operatorname{Re} \left[\frac{i}{\mu_1 - \mu_2} (q_2 - q_1) \right] \quad (23)$$

$$u_2 = K_I \sqrt{\frac{2r}{\pi}} \operatorname{Re} \left[\frac{i}{\mu_1 - \mu_2} (\mu_1 p_2 - \mu_2 p_1) \right] + K_{II} \sqrt{\frac{2r}{\pi}} \operatorname{Re} \left[\frac{i}{\mu_1 - \mu_2} (p_2 - p_1) \right] \quad (24)$$

Using Eqs. (21, 24) and Eqs. (22, 23), stress intensity factor formulas for pure Mode I (K_I) and Mode II (K_{II}) can be obtained.

$$K_I = \frac{1}{4} \sqrt{\frac{2\pi D(4\Delta u_{34} - \Delta u_{56}) - B(4\Delta v_{34} - \Delta v_{56})}{\Delta b}} \frac{AD - BC}{AD - BC} \quad (25)$$

$$K_{II} = \frac{1}{4} \sqrt{\frac{2\pi A(4\Delta v_{34} - \Delta v_{56}) - C(4\Delta u_{34} - \Delta u_{56})}{\Delta b}} \frac{AD - BC}{AD - BC} \quad (26)$$

where A , B , C and D are given as follows

$$A = \operatorname{Re} \left[\frac{i}{\mu_1 - \mu_2} (\mu_1 p_2 - \mu_2 p_1) \right] \quad (27)$$

$$B = \operatorname{Re} \left[\frac{i}{\mu_1 - \mu_2} (p_2 - p_1) \right] \quad (28)$$

$$C = \operatorname{Re} \left[\frac{i}{\mu_1 - \mu_2} (\mu_1 q_2 - \mu_2 q_1) \right] \quad (29)$$

$$D = \operatorname{Re} \left[\frac{i}{\mu_1 - \mu_2} (q_2 - q_1) \right] \quad (30)$$

3.2 Finite Element Model

The orthotropic FGM plate having center crack is modeled using *ANSYS* finite element package program for numerical solution and two dimensional *Plane82* is used as the element type (*ANSYS* 2009). *Plane82* provides more accurate results for mixed (quadrilateral-triangular) automatic meshes and can tolerate irregular shapes without much loss of accuracy. The 8-node *Plane82* element is defined by eight nodes having two degrees of freedom at each node: translations in the nodal X_1 and X_2 axes. The element may be used as a plane element or as an axisymmetric element. The element has plasticity, creep, swelling, stress stiffening, large deflection, and large strain capabilities.

The problem is solved by assuming as generalized plane stress. The numerical model is developed for four different boundary conditions. Boundary conditions of problem and dimensions of orthotropic FGM plate are given in Fig. 3. Plate dimensions are $a/W = 0.1$ and $L/W = 1.0$. All finite element models

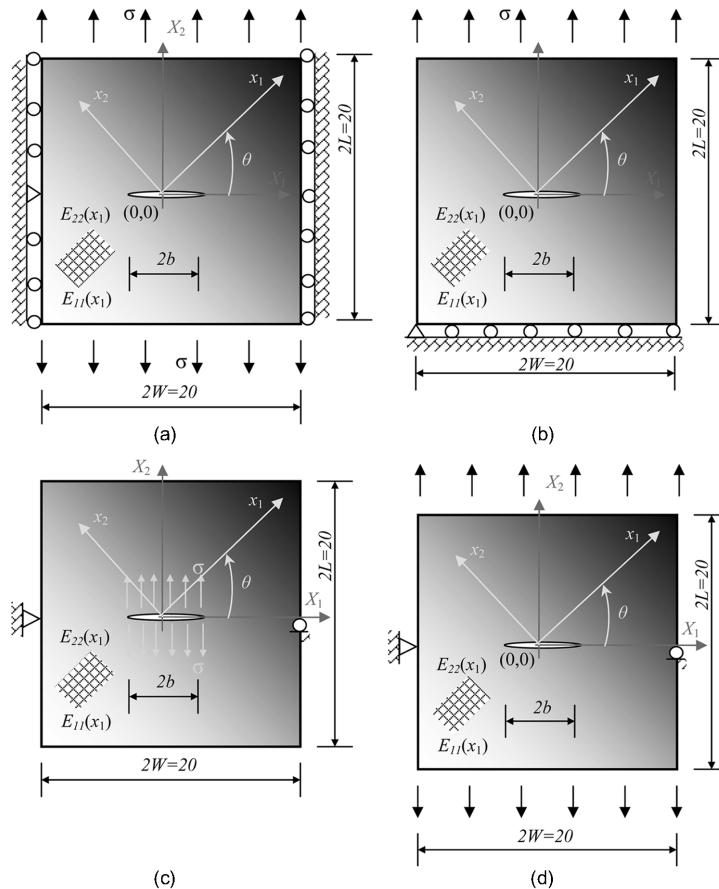


Fig 3 Dimensions of orthotropic FGM plate for four different boundary conditions; (a) Model 1, (b) Model 2, (c) Model 3, (d) Model 4

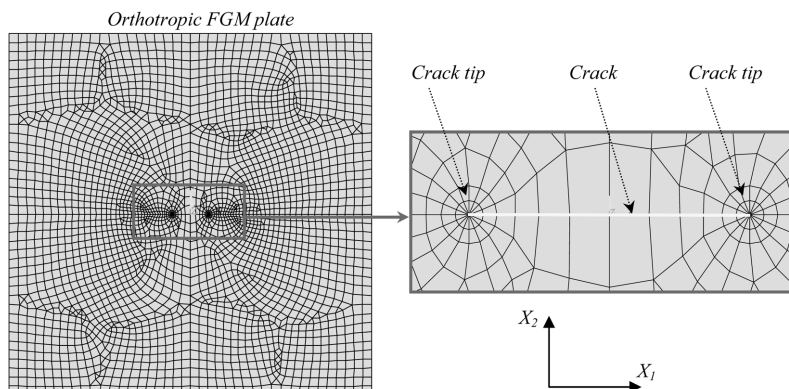


Fig 4 Finite element model of orthotropic FGM plate for *Plane82* element

consist of 2881 elements and 8649 nodes. As illustrated by Figs. 3(a)-(d), the variations of E_{11} , E_{22} , and G_{12} are assumed to be exponential functions of x_1 (Eqs. (1)-(3)) and proportional to one another, while the Poisson's ratio ν is constant. Note that the crack is not parallel to the material direction and the average Young's modulus is defined as $E \equiv E(X_1) = E^0 e^{(\phi_1 X_1 + \phi_2 X_2)}$ where $E^0 = \sqrt{E_{11}^0 E_{22}^0}$.

Figs. 3(a) and 3(b) show a crack of length $2b$ located in a finite two-dimensional plate under remote uniform tension loading for two different boundary conditions. The boundary conditions are defined such that $u_1 = 0$ along the left and right edges and $u_2 = 0$ for the node in the middle of the left edge as seen Fig. 3(a), $u_2 = 0$ along the bottom edge and $u_1 = 0$ at the left corner node of the bottom edge as seen Fig. 3(b) (Kim and Paulino 2002a).

Fig. 3(c) shows a crack of length $2b$ located in a finite two-dimensional plate under uniform crack pressure loading. The displacement boundary condition is defined such that $u_1 = u_2 = 0$ for the node in the middle of the left edge and $u_2 = 0$ for the node in the middle of the right edge. The applied load corresponds to $\pm\sigma$ ($-1 \leq X_1 \leq +1$) along the crack faces.

Fig. 3(d) shows a center crack of length $2b$ located in a finite two-dimensional plate under constant applied tension load. The applied load corresponds to $\pm\sigma$ ($-10 \leq X_1 \leq +10$, $X_2 = \pm 10$) along the top and bottom edges. The displacement boundary condition is prescribed such that $u_1 = u_2 = 0$ for the node in the middle of the left edge and $u_2 = 0$ for the node in the middle of the right edge. Fig. 4 shows finite element model of FGM plate.

3.3 The implementation of orthotropic FGMs to the finite element model

As *ANSYS* does not offer variation in assigned material properties across elements directly, the material property gradient is applied via a spatial variation in assigned nodal temperatures. As the finite element formulation leads to an interpolation of temperatures within the elements, this results in a continuous variation in properties (Rousseau and Tippur 2000). Therefore gradient of material properties for FGM are defined as a function of temperature with the help of a subroutine prepared by using APDL codes. Then the Young's modulus is defined as a linear function of temperature and the coefficient of thermal expansion is set to zero to avoid the presence of thermal residual stresses (Tilbrook *et al.* 2005). So it is provided that meaningful property of temperature does not physically remain and exponential variation of material properties E_{11} , E_{22} and G_{12} is defined with using temperature as shown in Fig. 5.

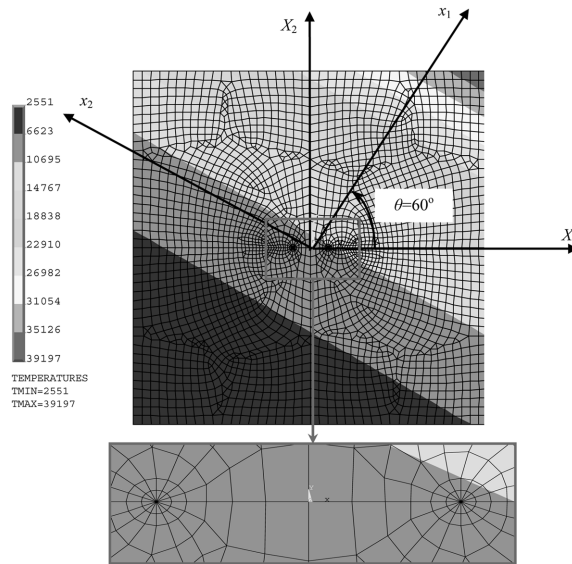


Fig 5 Applying of temperature distribution to the finite element model for $\beta = 0.1$, $\delta^4 = 4$, $\nu = 0.4$ and $\theta = 60^\circ$

4. Results and discussion

In this analysis, the effect of variation of angle θ° between material gradient $\mathbf{x}(x_1, x_2)$ and principal $\mathbf{X}(X_1, X_2)$ axes on stress intensity factor which is significant parameters of fracture analysis, is investigated for orthotropic FGM plate having center crack. On the other hand, effects of nonhomogeneity material parameter (βb), Poisson's ratio (ν), ratio of E_{11}/E_{22} (δ^4) and different boundary conditions with changing of θ° on stress intensity factor are examined by using finite element method, DCM.

The aim of this section is to determine numerically stress intensity factor of orthotropic FGM plates

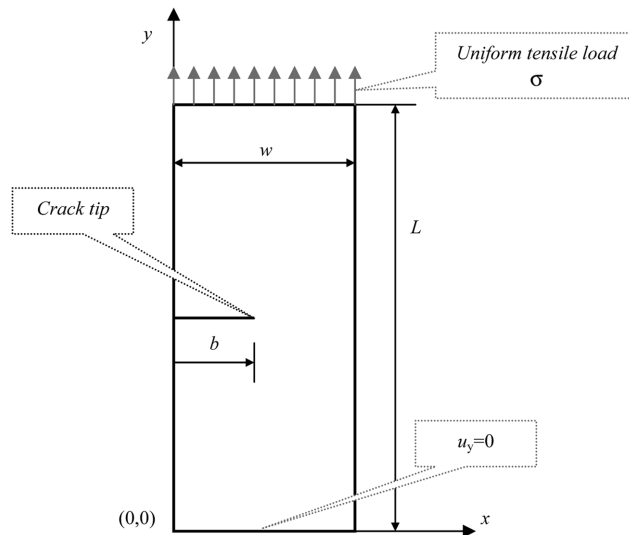


Fig 6 Dimensions and boundary conditions FGM plate having single edge crack

Table 1 Normalized stress intensity factors for FGM plate, $\bar{K}_I = K_I/(\sigma\sqrt{b\pi})$

E_2/E_1	Sladek <i>et al.</i>		Kim and Paulino	Present
	<i>LBIEM*</i>	<i>NASTRAN**</i>		<i>ANSYS</i>
1	2.108	2.110	-	2.113
0.2	2.400	2.420	2.431	2.431
2	1.970	1.960	-	1.959
5	1.740	1.760	1.749	1.749

**LBIEM* : Local boundary integral equation method

***NASTRAN* : Finite element package program

having center crack. To verify the solution technique, different analyses in references (Kim and Paulino 2002a, Kim and Paulino 2002b, Kim and Paulino 2003b, Ozturk and Erdogan 1997, Ozturk and Erdogan 1999, Sladek *et al.* 2005) are resolved with using *ANSYS*.

The first problem of analyses is a single edge cracked rectangular homogeneous FGM body subjected to tension as shown in Fig. 6. The dimensions of the body are $L = 30$ mm, $w = 10$ mm and $b/w = 0.4$. The *Plane82* element type is used in numerical model. The model consists of 1817 elements and 5546 nodes. Young's modulus of FGM body is

$$E(x) = E_1 e^{(\beta x)} \quad 0 \leq x \leq w \quad (31)$$

where the material parameters are $\beta = (1/w)\ln(E_2/E_1)$, $E_1 = E(0) = 10000$ MPa and $E_2 = E(2)$. The Poisson's ratio is. The single edge crack problem is solved with DCM. At the end of the solution, all given stress intensity factor values are normalized with (Table 1)

$$\bar{K}_I = \frac{K_I}{\sigma\sqrt{\pi b}} \quad (32)$$

$$\bar{K}_{II} = \frac{K_{II}}{\sigma\sqrt{\pi b}} \quad (33)$$

The second problem of analyses is a center cracked rectangular orthotropic FGM body subjected to fixed grip loading as shown in Fig. 7. The dimensions of the body are $L/W = 1.0$ and $b/w = 0.1$. The *Plane82* element type is used in numerical model. The model consists of 2881 elements and 8649 nodes. Center crack is parallel to the material gradation ($\theta = 0^\circ$). Material properties of FGM body are

$$E_{11}(X_1) = E_{11}^0 e^{\beta X_1} \quad (34)$$

$$E_{22}(X_1) = E_{22}^0 e^{\beta X_1} \quad (35)$$

$$G_{12}(X_1) = G_{12}^0 e^{\beta X_1} \quad (36)$$

where the material parameters are $\beta b = 0.5$, $\kappa_0 = 0.5$ and $\varepsilon_0 = 1.0$. The Poisson's ratio is $\nu = 0.2 = \text{constant}$. The single edge crack problem is solved with DCM. At the end of the solution, all given stress intensity factor values are normalized with Eqs. (32), (33). The normalized stress intensity factor results are

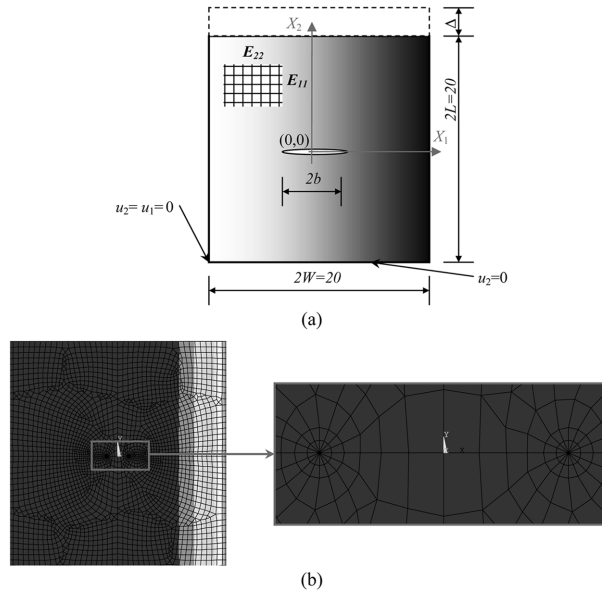


Fig 7 (a) Orthotropic FGM plate with a crack parallel to the material gradation under fixed grip loading, (b) finite element model

Table 2 Normalized SIFs in an non-homogeneous orthotropic plate under fixed grip loading ($K_0 = \varepsilon_0 \bar{E}^0 \sqrt{\pi b}$, $\bar{E}^0 = E^0 / \delta^0$, $E^0 = \sqrt{E_{11}^0 E_{22}^0}$)

ν	Ozturk and Erdogan		Kim and Poulino		Present	
	$K_I(+b)/K_0$	$K_I(-b)/K_0$	$K_I(+b)/K_0$	$K_I(-b)/K_0$	$K_I(+b)/K_0$	$K_I(-b)/K_0$
0.1	1.4183	0.6647	1.4451	0.6776	1.4438	0.6849
0.2	1.4233	0.6676	1.4488	0.6802	1.4484	0.6881
0.3	1.4280	0.6704	1.4522	0.6822	1.4527	0.6911
0.4	1.4325	0.6730	1.4559	0.6843	1.4567	0.6939
0.5	1.4368	0.6755	1.4593	0.6864	1.4605	0.6965
0.7	1.4449	0.6802	1.4655	0.6902	1.4669	0.7013
0.9	1.4524	0.6846	1.4718	0.6939	1.4696	0.7045

compared with available literature as seen in Table 2. There are negligible differences between the present study and the references for both homogeneous and orthotropic FGM plate problems.

Attention will first be focused on the results of Model 1 (Fig. 3(a)). Variations of normalized Mode I and II stress intensity factors at the $-b$ and $+b$ edges of center crack in a rectangular orthotropic FGM plate are shown in Figs. 8 and 9. Fig. 8 shows variation of $\bar{K}_I(+b)$ and $\bar{K}_{II}(+b)$ and with material angle θ° for $\nu = 0.2$, $\kappa_0 = 0.5$, $\delta^4 = E_{11}/E_{22} = 4$. It is seen that $\bar{K}_I(+b)$ assumes its minimum value at $\theta = 0^\circ$. This effect is most pronounced for greater values of βb . The effect of non homogeneity parameter βb is greater when θ is smaller. On the other hand, maximum values of $\bar{K}_{II}(+b)$ are obtained at $\theta = 45^\circ$ and increases with increasing βb . is equal to the zero for all βb values for $\theta = 0^\circ$, because there is pure Mode I state at this angle. $\bar{K}_I(-b)$ and $\bar{K}_{II}(-b)$ show the same behavior with $\bar{K}_I(+b)$ and $\bar{K}_{II}(+b)$, respectively. But $\bar{K}_I(+b)$ values are greater than that of $\bar{K}_I(-b)$. This is expected due to the nature of the exponential material gradation with the origin of the cartesian coordinate system at the

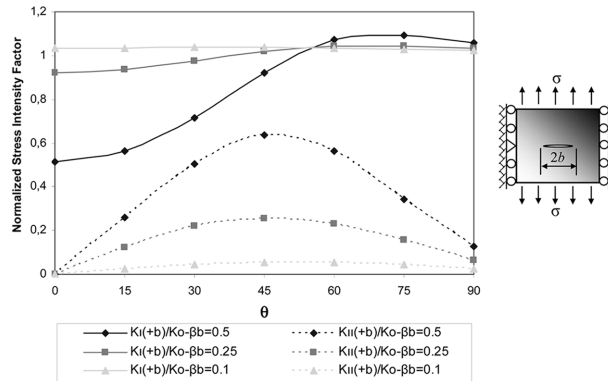


Fig 8 Normalized stress intensity factor when $\nu = 0.2, \kappa_0 = 0.5, \delta^d = 4$

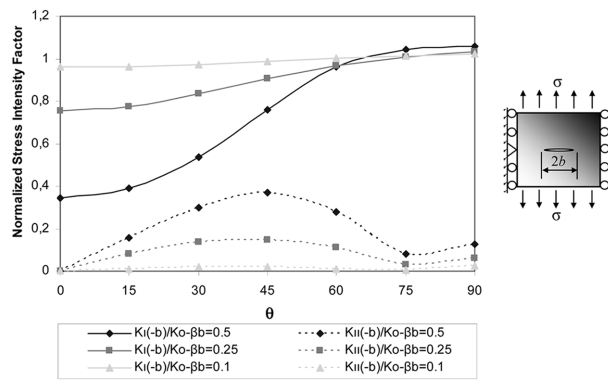


Fig 9 Normalized stress intensity factor when $\nu = 0.2, \kappa_0 = 0.5, \delta^d = 4$

center of the plate.

Figs. 10 and 11 show variation of $\bar{K}_I(+b), \bar{K}_{II}(+b)$ and $\bar{K}_I(-b), \bar{K}_{II}(-b)$ with material angle θ° when $\beta b = 0.25, \kappa_0 = 0.5, \delta^d = E_{11}/E_{22} = 4$ for Model 1, respectively. The effect of variation of $\nu = \sqrt{v_{12}v_{21}}$ on stress intensity factor is very small and $\bar{K}_I(+b)$ increases with increasing ν at $\theta = 0^\circ$. This effect decreases with increasing θ . At $\theta = 90^\circ$, there is no Poisson's effect on $\bar{K}_I(+b)$. In addition to this, $\bar{K}_{II}(+b)$ values do not change with changing ν at all material angles. These effects and behaviors

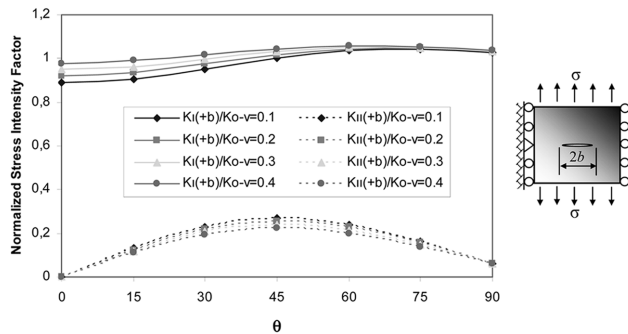


Fig 10 Normalized stress intensity factor when $\beta b = 0.25, \kappa_0 = 0.5, \delta^d = 4$

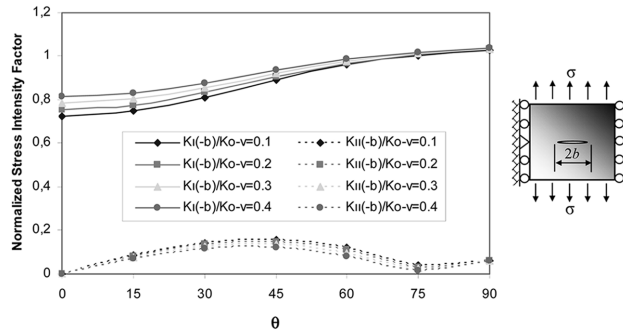


Fig 11 Normalized stress intensity factor when $\beta b = 0.25$, $\kappa_0 = 0.5$, $\delta^4 = 4$

are valid for $\bar{K}_I(-b)$ and $\bar{K}_{II}(-b)$ (Fig. 11).

Figs. 12-14 show variations of $\bar{K}_I(+b)$ and $\bar{K}_I(-b)$ with θ when $\nu = 0.2$, $\kappa_0 = 0.5$, $\delta^4 = 4$ for $\beta b = 0.5, 0.25$ and 0.1 , respectively (Model 2). As can be seen in these figures, the effect of variation of θ on SIFs decreases with decreasing βb . $\bar{K}_I(+b)$ values are greater than that of $\bar{K}_I(-b)$ for all βb values. Maximum normalized stress intensity factor is obtained by $\bar{K}_I(+b) = 1.967$ when $\theta = 45^\circ$, $\beta b = 0.5$, $\nu = 0.2$, $\kappa_0 = 0.5$, $\delta^4 = 4$ (Fig. 12). $\bar{K}_I(+b)$ and $\bar{K}_I(-b)$ increase by up to 45° , then decrease when $\beta b = 0.5$. But and always decreases with increasing θ when $\beta b = 0.25$. This decreasing is very small, in the other words, the effect of βb is almost non-existent for $\beta b = 0.1$. For all βb values, $\bar{K}_I(+b)$ and $\bar{K}_I(-b)$, $\bar{K}_{II}(+b)$ and $\bar{K}_{II}(-b)$ are equal to each other at the $\theta = 90^\circ$. For the reason of this situation it can be said that material properties are the same at two crack tips ($\pm b, 0$) for this angle.

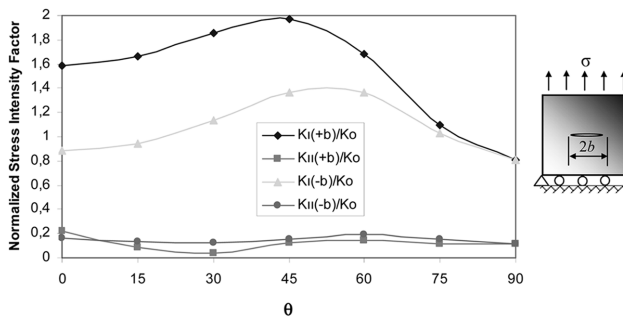


Fig 12 Normalized stress intensity factor when $\beta b = 0.5$, $\nu = 0.2$, $\kappa_0 = 0.5$, $\delta^4 = 4$

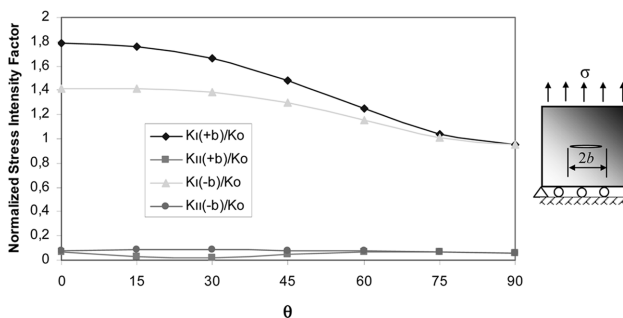


Fig 13 Normalized stress intensity factor when $\beta b = 0.25$, $\nu = 0.2$, $\kappa_0 = 0.5$, $\delta^4 = 4$

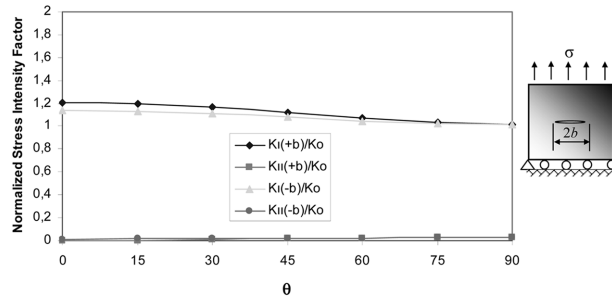


Fig 14 Normalized stress intensity factor when $\beta b = 0.1, \nu = 0.2, \kappa_0 = 0.5, \delta^4 = 4$

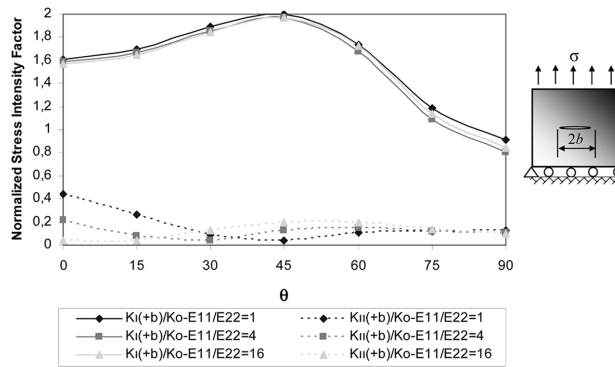


Fig 15 Normalized stress intensity factor when $\beta b = 0.5, \nu = 0.2, \kappa_0 = 0.5$

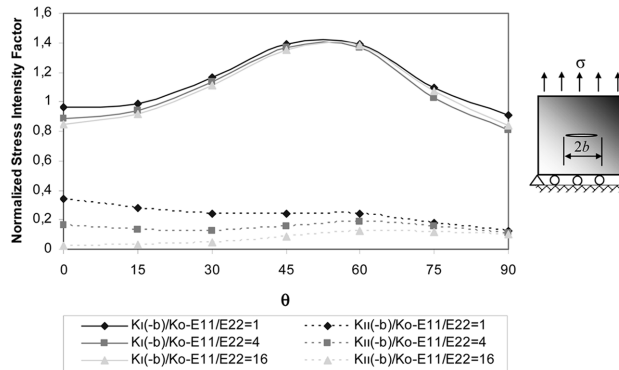


Fig 16 Normalized stress intensity factor when $\beta b = 0.5, \nu = 0.2, \kappa_0 = 0.5$

Figs. 15 and 16 show the effect of $\delta^4 = E_{11}/E_{22}$ on normalized SIF when $\beta b = 0.5, \nu = 0.2, \kappa_0 = 0.5$. δ^4 has a negligible effect on the $\bar{K}_I(+b)$ and $\bar{K}_I(-b)$. On the other hand, $\bar{K}_{II}(+b)$ and $\bar{K}_{II}(-b)$ increase with decreasing E_{11}/E_{22} at $\theta = 0^\circ$. For all δ^4 , $\bar{K}_{II}(+b)$ and $\bar{K}_{II}(-b)$ values are very close to each other at $\theta = 90^\circ$.

Now, attention will be focused on the results of Model 3 (Fig. 3(c)). To verify the solution technique for orthotropic FGM, an analysis is resolved in references (Fig. 17). Center crack is perpendicular to the material gradation ($\theta = 90^\circ$). Material properties of FGM body are

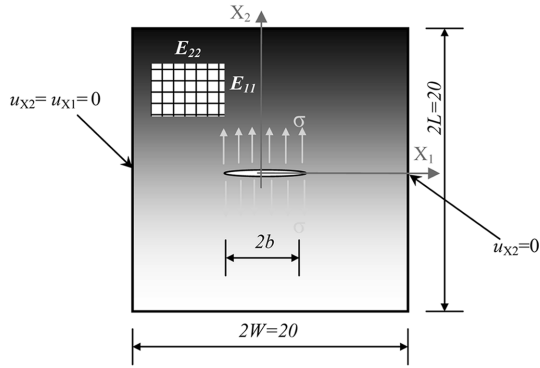


Fig 17 Orthotropic FGM plate with a crack perpendicular to the material gradation under uniform crack pressure loading

Table 3 Normalized SIFs in a non-homogeneous orthotropic plate with crack face pressure loading ($\kappa_0 = 5.0$, $K_0 = \sigma\sqrt{\pi b}$, $\delta^4 = 10$)

βb	ν	Ozturk and Erdogan		Kim and Poulino		Present	
		$K_I(+b)/K_0$	$K_{II}(+b)/K_0$	$K_I(+b)/K_0$	$K_{II}(+b)/K_0$	$K_I(+b)/K_0$	$K_{II}(+b)/K_0$
0.5	0.15	1.0748	0.1252	1.0820	0.1143	1.0892	0.1198
	0.30	1.0776	0.1252	1.0840	0.1144	1.0927	0.1199
	0.45	1.0804	0.1251	1.0860	0.1144	1.0960	0.1201
1.0	0.15	1.1892	0.2511	1.1960	0.2273	1.2001	0.2400
	0.30	1.1955	0.2512	1.1994	0.2274	1.2069	0.2404
	0.45	1.2017	0.2512	1.2051	0.2274	1.2135	0.2408

$$E_{11}(X_2) = E_{11}^0 e^{\beta X_2} \quad (37)$$

$$E_{22}(X_2) = E_{22}^0 e^{\beta X_2} \quad (38)$$

$$G_{12}(X_2) = G_{12}^0 e^{\beta X_2} \quad (39)$$

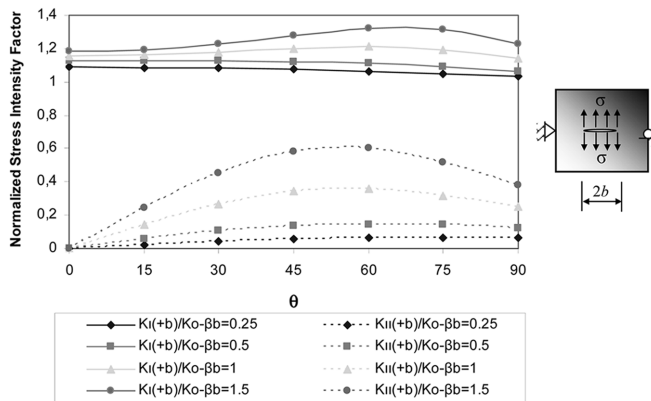


Fig 18 Normalized stress intensity factor when $\nu = 0.2$, $\kappa_0 = 0.5$, $\delta^4 = 4$

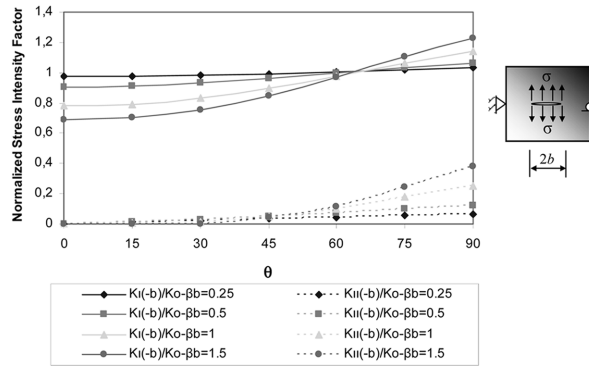


Fig 19 Normalized stress intensity factor when $\nu = 0.2, \kappa_0 = 0.5, \delta^4 = 4$

Obtained compatible results are given in Table 3. Figs. 18 and 19 show variation of normalized SIF with θ for different βb when $\nu = 0.2, \kappa_0 = 0.5, \delta^4 = 4$. $\bar{K}_I(+b)$ and $\bar{K}_{II}(+b)$ increase by up to $\theta = \sim 60^\circ$, then decrease for $\beta b > \sim 0.5$. The normalized SIFs $\bar{K}_I(+b)$ and $\bar{K}_{II}(+b)$ increase with increasing βb for all θ except for at $\theta = 0^\circ$ (Fig. 18). But $\bar{K}_I(-b)$ increases with decreasing βb by up to $\theta = \sim 60^\circ$, then increases. There is no effect of βb on $\bar{K}_{II}(-b)$ and $\bar{K}_{II}(+b)$ at $\theta = 0^\circ$ ($\bar{K}_{II}(-b)$ and $\bar{K}_{II}(+b) = 0$ for all

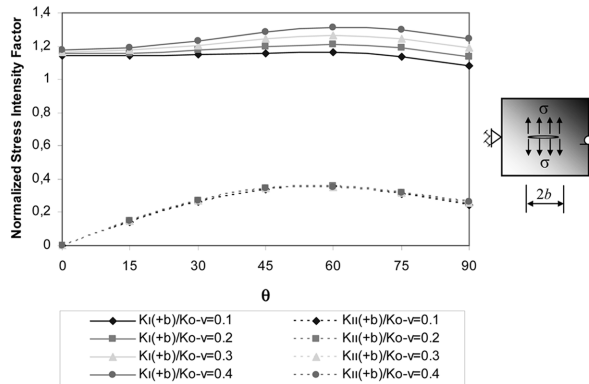


Fig 20 Normalized stress intensity factor when $\beta b = 1, \nu_{12} = 0.4, \kappa_0 = 0.5$

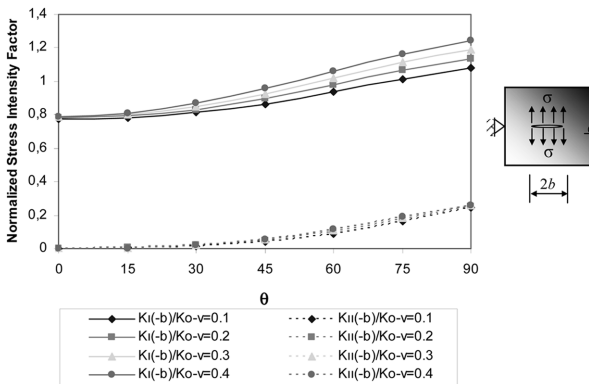


Fig 21 Normalized stress intensity factor when $\beta b = 1, \nu_{12} = 0.4, \kappa_0 = 0.5$

Table 4. Normalized stress intensity factor for Model-4 when $\nu = 0.2$, $\delta^t = 4$

βb	θ ($^\circ$)	$\kappa_0 = 0.5$				$\kappa_0 = 0.5$			
		$K_{I(+b)}/K_0$	$K_{II(+b)}/K_0$	$K_{I(-b)}/K_0$	$K_{II(-b)}/K_0$	$K_{I(+b)}/K_0$	$K_{II(+b)}/K_0$	$K_{I(-b)}/K_0$	$K_{II(-b)}/K_0$
0.5	0	1.61123	0.00039	0.92427	0.00033	1.41996	0.00076	1.00645	0.00080
	15	1.67078	0.20736	0.99043	0.09342	1.42015	0.15790	1.03115	0.06724
	30	1.79295	0.36837	1.16199	0.15288	1.40804	0.22546	1.07922	0.06864
	45	1.79650	0.39571	1.31927	0.12162	1.36422	0.21422	1.11482	0.01475
	60	1.49288	0.26352	1.25989	0.00427	1.26833	0.16919	1.11307	0.05450
	75	1.02097	0.12702	0.97275	0.10740	1.12615	0.12855	1.06254	0.10287
	90	0.79719	0.10825	0.79721	0.10805	1.03423	0.11516	1.03407	0.11584
0.25	0	1.73827	0.00044	1.38984	0.00049	1.36796	0.00078	1.16243	0.00088
	15	1.70508	0.05014	1.38031	0.00635	1.35020	0.03588	1.15716	0.00075
	30	1.60069	0.08217	1.34192	0.00130	1.29959	0.05876	1.14014	0.00863
	45	1.42458	0.08766	1.25662	0.01752	1.22385	0.06651	1.10965	0.02484
	60	1.20919	0.07547	1.12717	0.04104	1.13708	0.06498	1.06886	0.04265
	75	1.02702	0.06347	1.00055	0.05593	1.06225	0.06175	1.03225	0.05486
	90	0.95109	0.05985	0.95115	0.05968	1.02460	0.05949	1.02440	0.05990
0.1	0	1.19405	0.00030	1.12820	0.00040	1.11708	0.00065	1.06251	0.00078
	15	1.18285	0.00816	1.12077	0.00506	1.11187	0.00805	1.05976	0.00602
	30	1.15184	0.01526	1.09995	0.01055	1.09740	0.01449	1.05219	0.01125
	45	1.10837	0.02028	1.07032	0.01579	1.07700	0.01939	1.04177	0.01618
	60	1.06335	0.02326	1.03957	0.02018	1.05540	0.02260	1.03167	0.02035
	75	1.02840	0.02463	1.01734	0.02316	1.03760	0.02425	1.02569	0.02326
	90	1.01219	0.02467	1.01227	0.02455	1.02734	0.02440	1.02712	0.02464

βb values). But $\bar{K}_{II}(-b)$ increases with increasing θ . At the $\theta = 90^\circ$, maximum values of SIF obtained for $\beta b = 1.5$ ($\bar{K}_{II}(-b) = 0.382$). Figs. 20 and 21 show the effect of Poisson's ratio on normalized SIFs when $\beta b = 1$, $\nu_{12} = 0.4$, $\kappa_0 = 0.5$. $\bar{K}_{II}(+b)$ and $\bar{K}_{II}(-b)$ are completely insensitive to ν . $\bar{K}_{I}(+b)$ increases with increasing ν at $\theta = 90^\circ$. This effect decreases with decreasing θ . At the $\theta = 0^\circ$, there is no effect of ν on normalized SIFs $\bar{K}_{I}(+b)$ and this behavior is valid for $\bar{K}_{I}(-b)$ (Fig. 21).

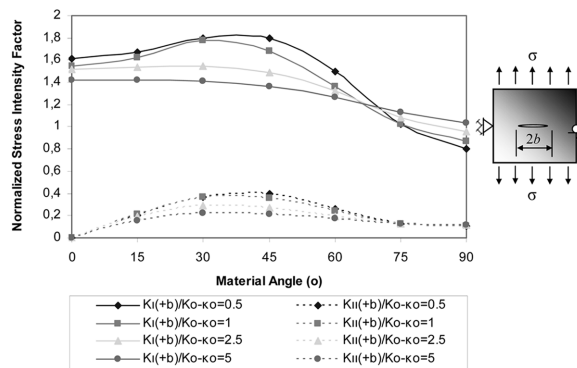


Fig 22 Normalized stress intensity factor when $\beta b = 0.5$, $\nu = 0.2$, $\delta^t = 4$

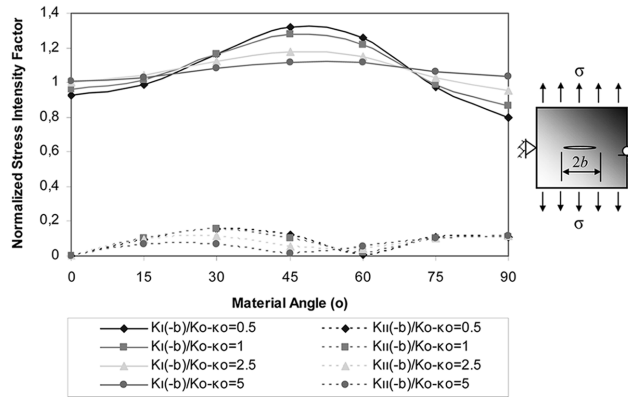


Fig 23 Normalized stress intensity factor when $\beta b = 0.5, \nu = 0.2, \delta^4 = 4$

In this stage, numerical results are examined for Model 4. Table 4 gives the effect of βb on normalized SIF for different angles θ when $\nu = 0.2, \delta^4 = 4$. As can be seen in this table, the effect of variation of θ on SIFs decreases with decreasing βb as in Model 2. Figs. 22 and 23 give variation of normalized SIFs with q for different κ_0 when $\beta b = 0.5, \nu = 0.2, \delta^4 = 4$. The effect of θ on SIFs decreases with increasing κ_0 . $\bar{K}_I(+b)$ values are greater than $\bar{K}_{II}(-b)$. $\bar{K}_I(+b)$ increases with decreasing κ_0 for $\theta < \sim 65^\circ$ and increasing κ_0 for $\theta > \sim 65^\circ$. $\bar{K}_{II}(+b)$ and $\bar{K}_{II}(-b)$ are equal to the zero for all κ_0 at the $\theta = 0^\circ$. $\bar{K}_I(-b)$ increases with decreasing κ_0 for $\sim 25^\circ < \theta < \sim 65^\circ$. The outside of this range, the opposite behavior is valid for $\bar{K}_I(-b)$.

Figs. 24 and 25 show normalized SIFs in a non-homogeneous orthotropic plate under uniform tension for four different boundary conditions for a fixed stiffness ratio $\delta^4 = 4$ and constant Poisson's ratio $\nu = 0.2$ with material nonhomogeneity $\beta b = 0.5$. This figure clearly indicates that the boundary conditions have a significant influence on SIFs. The normalized SIFs values $\bar{K}_I(+b)$ of Model 1 and Model 3 are ~ 0.79 at $\theta = 90^\circ$. Additionally, these values are ~ 1.06 for Model 2 and Model 4. This situation is caused by having similar boundary conditions between the models. The similar behavior of the SIF values can be obtained for $\bar{K}_I(-b)$.

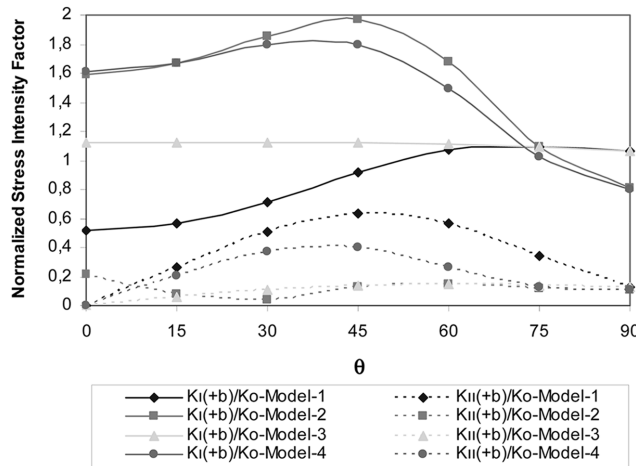


Fig 24 Normalized stress intensity factor when $\beta b = 0.5, \nu = 0.2, \kappa_0 = 0.5, \delta^4 = 4$

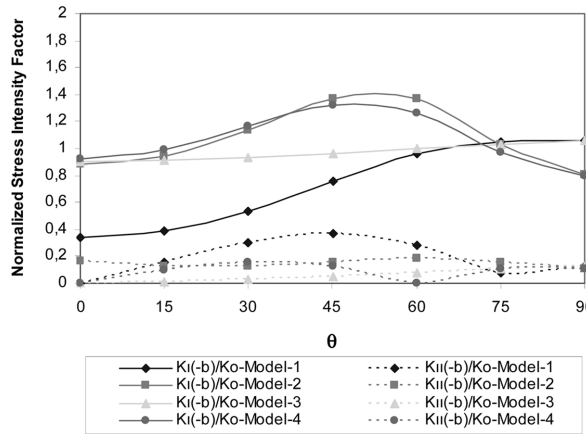


Fig 25 Normalized stress intensity factor when $\beta b = 0.5$, $\nu = 0.2$, $\kappa_0 = 0.5$, $\delta^4 = 4$

5. Conclusion

This study represents numerical SIF results of orthotropic FGM plate having center crack the axis and exponential material axis of which differ by θ° . Besides, effects of nonhomogeneity material parameter (βb), Poisson’s ratio (ν), ratio of E_{11}/E_{22} (δ^4) and different boundary conditions with changing of θ° on stress intensity factor are investigated by using displacement correlation method. The concluded points may be listed as follow:

- The non-homogeneous parameter (βb) determines the effect of variation of angle θ° between material gradient $x(x_1, x_2)$ and principal $X(X_1, X_2)$ axes on stress intensity factor for different boundary conditions. The effect of θ° on SIF increases with the increase in βb for all models, namely boundary conditions.
- The effect of variation of $\nu = \sqrt{v_{12}v_{21}}$ on stress intensity factor is very small and $\bar{K}_{I(+b)}$ increases with the increase of ν at $\theta = 0^\circ$ for Model 1. This effect decreases with the increase of θ . There is no Poisson’s effect on $\bar{K}_{I(+b)}$ at $\theta = 90^\circ$.
- δ^4 has a negligible effect on the $\bar{K}_{I(+b)}$ and $\bar{K}_{I(-b)}$ for Model 2. On the other hand, $\bar{K}_{II(+b)}$ and $\bar{K}_{II(-b)}$ increase with the decrease in E_{11}/E_{22} at $\theta = 0^\circ$ and are very close to each other at $\theta = 90^\circ$.
- The effect of Poisson’s ratio is investigated on normalized SIF values when $v_{12} = constant$ for Model 3. $\bar{K}_{II(+b)}$ and $\bar{K}_{II(-b)}$ are completely insensitive to ν . $\bar{K}_{I(+b)}$ and $\bar{K}_{I(-b)}$ increase with the increase of ν at $\theta = 90^\circ$. This effect decreases with the decrease of θ . There is no effect of ν on normalized SIFs when $v_{12} = constant$ at the $\theta = 0^\circ$.
- The variation of normalized SIF values with κ_0 for different angles is investigated for Model 4. It can be said that, the effect of θ° on SIF values decreases with an increase in κ_0 .
- The boundary conditions have a significant influence on SIF values and this situation changes the effect of θ on SIFs, too.
- The gradient of material properties for orthotropic FGM is defined as a function of temperature with the help of a subroutine prepared by using APDL codes. The negligible differences are obtained between the results of present study using this technique and the references. This result is very important since it can easily provide prediction of more complex models.
- The numerical solution technique DCM is easily applicable method. Besides this method, the analysis can be expanded by the application of the M integral and displacement extrapolation methods.

References

- ANSYS 12.1 (2009), *Academic Teaching Introductory Help Menu*.
- Ayhan, A.O. (2007), "Stress intensity factors for three-dimensional cracks in functionally graded materials using enriched finite elements", *Int. J. Solids Struct.*, **44**(25-26), 8579-8599.
- Chalivendra, V.B. (2009), "Mixed-mode crack-tip stress fields for orthotropic functionally graded materials", *ACTA Mech.*, **204**(1-2), 51-60.
- Chen, J., Liu, Z., and Zou, Z. (2002), "Transient internal crack problem for a nonhomogeneous orthotropic strip (Mode I)", *Int. J. Eng. Sci.*, **40**(15), 1761-1774.
- Dag, S. (2006), "Thermal fracture analysis of orthotropic functionally graded materials using an equivalent domain integral approach", *Eng. Fract. Mech.*, **73**(18), 2802-2828.
- Dag, S., Yildirim, B., and Sarikaya, D. (2007), "Mixed-mode fracture analysis of orthotropic functionally graded materials under mechanical and thermal loads", *Int. J. Solids Struct.*, **44**(24), 7816-7840.
- Gao, X., Zhang, Ch., Sladek, J., Sladek, V. (2008), "Fracture analysis of functionally graded materials by a BEM", *Compos Sci Technol*, **68**(5), 1209-1215.
- Guo, L.C., Wu, L.Z., Zeng, T., and Ma, L. (2004), "Mode I crack problem for a functionally graded orthotropic strip", *Eur. J. Mech. A Solids*, **23**(2), 219-234.
- Hongmin, X., Xuefeng, Y., Xiqiao, F., and Yeh, H.Y. (2008), "Dynamic stress intensity factors of a semi-infinite crack in an orthotropic functionally graded material", *Mech. Mater.*, **40**(1-2), 37-47.
- Kim, J.H. and Paulino, G.H. (2002a), "Mixed-mode fracture of orthotropic functionally graded materials using finite elements and the modified crack closure method", *Eng. Fract. Mech.*, **69**(14-16), 1557-1586.
- Kim, J.H. and Paulino, G.H. (2002b), "Finite element evaluation of mixed mode stress intensity factors in functionally graded materials", *Int. J. Numer. Methods Eng.*, **53**, 1903-1935.
- Kim, J.H. and Paulino, G.H. (2003a), "The interaction integral for fracture of orthotropic functionally graded materials: evaluation of stress intensity factors", *Int. J. Solids Struct.*, **40**(15), 3967-4001.
- Kim, J.H. and Paulino, G.H. (2003b), "Mixed-mode J-integral formulation and implementation using graded elements for fracture analysis of nonhomogeneous orthotropic materials", *Mech. Mater.*, **35**(1-2), 107-128.
- Kim, J.H. and Paulino, G.H. (2005), "Consistent formulations of the interaction integral method for fracture of functionally graded materials", *J. Appl. Mech.*, **72**(3), 351-364.
- Ozturk, M. and Erdogan, F. (1997), "Mode I crack problem in an inhomogeneous orthotropic medium", *Int. J. Numer. Eng. Sci.*, **35**(9), 869-883.
- Ozturk, M. and Erdogan, F. (1999), "The mixed mode crack problem in an inhomogeneous orthotropic medium", *Int. J. Fract.*, **98**(3-4), 243-261.
- Rao, B.N. and Rahman, S. (2003), "An interaction integral method for analysis of cracks in orthotropic functionally graded materials", *Comput. Mechanics*, **32**(1-2), 40-51.
- Rousseau, C.E. and Tippur, H.V. (2000), "Compositionally graded materials with cracks normal to the elastic gradient", *ACTA Mater.*, **48**(16), 4021-4033.
- Shih, C.F., Lorenzi, H.G., and German, M.D. (1976), "Crack extension modeling with singular quadratic isoparametric elements", *Int. J. Fracture*, **12**(4), 647-651.
- Sills, L.B., Hershkovitz, I., Wawrzynek, P.A., Eliasi, R., and Ingrassia, A.R. (2005), "Methods for calculating stress intensity factors in anisotropic materials: part I-z = 0 is a symmetric plane", *Eng. Fract. Mech.*, **72**(15), 2328-2358.
- Sladek, J., Sladek, V., and Zhang, C. (2005), "An advanced numerical method for computing elastodynamic fracture parameters in functionally graded materials", *Comp. Mater. Sci.*, **32**(3-4), 532-543.
- Sladek, J., Sladek, V., Zhang, Ch. (2008a), "Evaluation of the stress intensity factors for cracks in continuously nonhomogeneous solids, part I: Interaction integral", *Mech Adv Mater Struc*, **15**, 438-443.
- Sladek, J., Sladek, V., Zhang, Ch. (2008b), "Evaluation of the stress intensity factors for cracks in continuously nonhomogeneous solids, part II: Meshless method", *Mech Adv Mater Struc*, **15**, 444-452.
- Tilbrook, M.T., Moon, R.J., and Hoffinan, M. (2005), "Finite element simulations of crack propagation in functionally graded materials under flexural loading", *Eng. Fract. Mech.*, **72**(16), 2444-2467.
- Zhou, Y.T., Li, X., and Qin, J.Q. (2007), "Transient thermal stress analysis of orthotropic functionally graded materials with a crack", *J. Therm. Stresses*, **30**(12), 1211-1231.